

PAPER • OPEN ACCESS

Synthesis and Characterisation of Copper Substituted Cobalt Ferrite Nanoparticles by Sol-Gel Auto Combustion Route

To cite this article: A Anugraha *et al* 2019 *IOP Conf. Ser.: Mater. Sci. Eng.* **577** 012059

View the [article online](#) for updates and enhancements.

You may also like

- [Temperature annealing dependence of structural, magnetic, and antibacterial properties of silver substituted cobalt ferrite nanoparticles produced by coprecipitation route](#)
Riyatun, Triana Kusumaningsih, Agus Supriyanto et al.
- [Cation trivalent tune of crystalline structure and magnetic properties in coprecipitated cobalt ferrite nanoparticles](#)
Nurdiyantoro Putra Prasetya, Riyana Indah Setiyani, Utari et al.
- [Magnetic properties of CoFe₂O₄ nanoparticle synthesized by salt-assisted sol-gel auto-combustion method](#)
M Khodaei and S Fayazadeh



ECS
The
Electrochemical
Society
Advancing solid state &
electrochemical science & technology

DISCOVER
how sustainability
intersects with
electrochemistry & solid
state science research

Synthesis and Characterisation of Copper Substituted Cobalt Ferrite Nanoparticles by Sol-Gel Auto Combustion Route

A Anugraha, V K Lakshmi, Gangothri S Kumar, T Raguram and K S Rajni*

Dept. of Sciences, Amrita School of Engineering, Coimbatore,
Amrita Vishwa Vidyapeetham, India

*E-mail: ks_rajani@cb.amrita.edu

Abstract. In the present study, the structural, functional, morphological and magnetic characteristics of copper substituted cobalt ferrite nanoparticles were investigated. The samples of $\text{Co}_{1-x}\text{Cu}_x\text{Fe}_2\text{O}_4$ at $x = 0.06, 0.08$ and 0.1 M were prepared by Sol-gel auto combustion route. X-ray diffraction technique was used to confirm the phase formation and structural analysis which matches with the JCPDS Data. The average crystallite size was found to be $\sim 25, \sim 19$ and ~ 18 nm for $x = 0.06, 0.08$ and 0.1 respectively. The Micro Raman Spectroscopy revealed the stretching vibrations at $274 \text{ cm}^{-1}, 660 \text{ cm}^{-1},$ and 466 cm^{-1} , which are characteristic of Spinel Ferrites. From the FTIR analysis, the band observed at 3457 cm^{-1} and 1650 cm^{-1} is assigned to hydrogen bonded O-H group and ionic stretching of C-H bond. The band assigned at 1105 cm^{-1} is due to Co – O and Cu - O or Fe – O vibrations. The existence of water adsorption band and metal oxygen band confirms the existence of Co and Cu in the synthesized sample. The surface morphology of samples was imaged by the field emission scanning electron microscope. The substitution of Cu^{2+} in the parent systems caused a significant reduction in particle size. The compositional analysis was done, which confirmed that the concentration of copper was increased in the samples. The samples were subjected to magnetic characterization because magnetic behavior is also affected by substitution of Copper in Cobalt ferrite. Magnetic hysteresis study at room temperature confirmed the reduction in saturation magnetization ($M_S = 14.25$ to 8.33 emu/g.) and reduction in coercivity ($H_C = 602.64$ to 380.94 Oe) when size is reduced. As the concentration of Cu into CoFe_2O_4 matrix increases, particle size decreases and the saturation magnetization decreases.

1. Introduction

Spinel ferrites have attracted very much attention because of their electronic, catalytic and magnetic properties. Magnetic properties of spinel ferrites are controlled by their crystallite size and hence during the preparation process of magnetic nanoparticles, the parameters such as particle size, sintering temperature, doping ratio, chemical ratio of components are given importance. Cobalt ferrite, a hard magnetic ferrite is most abundant and important magnetic nanoparticles with large magnetic anisotropy, and moderate saturation magnetization, makes it suitable for applications in magnetic recording [1], magneto-optical devices[2], magnetic resonance imaging[3], ferrofluid technology [4], drug delivery [5], biosensors [6]. They can be used in medical applications such as, hyperthermia, magnetic resonance imaging (MRI) and drug delivery. Copper ferrite is a spinel ferrite which exist both in tetragonal and cubic structure. The tetrahedral phase of copper ferrite has an inverse spinel structure which changes to a spinel cubic structure when subjected to a temperature above 360°C . Cobalt ferrite has an inverse spinel structure and copper ferrite has a spinel structure at temperatures greater than 360°C . Hence, when copper is doped in cobalt ferrite, copper gets in between the remaining unfilled tetrahedral and



octahedral sites. Therefore, Cu-doping in CoFe_2O_4 can give some mixed spinel structures depending upon the concentration of the constituent species [7]. The copper substitution further improves the properties by reducing the saturation magnetization and coercivity which in turn reduces the eddy current loss and thereby making it suitable for many more applications. The synthesis of copper substituted cobalt ferrite includes sonochemical reactions, microwave plasma, microemulsion [8], sol-gel synthesis [9], hydrothermal synthesis [10], solvothermal [11], co-precipitation [12], electrochemical [13], and combustion methods [14].

2. Experimental Technique

2.1. Preparation of Cu substituted Cobalt Ferrite Nanoparticles

In the present work copper substituted cobalt ferrites are prepared by sol-gel technique. The precursors are cobalt nitrate, citric acid monohydrate, copper nitrate and ferric nitrate. A suitable molar concentration of all these powders are dissolved in 100ml of distilled water separately and mixed together to prepare $\text{Co}_{(1-x)}\text{Cu}_x\text{Fe}_2\text{O}_4$ with $x = 0.06, 0.08$ and 0.1 M. The pH is maintained at 8 by adding ammonium hydroxide and its continuously stirred at $70-80^\circ\text{C}$ until a brown fluffy gel is obtained. Then the gel is annealed at 800°C for 2 hours to obtain a black powder and is grinded to get the powder.

2.2. Characterisation Technique

The samples were subjected to Powder X-ray diffraction analysis using Shimadzu XRD 6000 diffractometer with $\text{CuK}\alpha$ radiation of wavelength 1.541 \AA . The functional group was analyzed by FTIR using Perkin-Elmer spectrometer by KBr pellet technique in the range of $4000-400 \text{ cm}^{-1}$. The structure and its corresponding vibrational modes were confirmed using Micro-Raman Spectroscopy (Renishaw Raman Microscope (RE04)). The morphology analysis of the prepared samples was assessed by Scanning Electron microscopy using JEOL (JSM 6390). Magnetic properties of the samples were analyzed by VSM (Lakeshore VSM 7410 equipped with an electromagnet) at room temperature with the maximum applied field of 15kOe .

3. Results and Discussion

3.1. Structural Analysis

The structural analysis of $\text{Co}_{1-x}\text{Cu}_x\text{Fe}_2\text{O}_4$ ($x = 0.06, 0.08$ and 0.1) is carried out by XRD (Figure 1). The diffraction peaks corresponding to the planes (2 2 0), (3 1 1), (2 2 2), (4 0 0), (4 2 2), (5 1 1), (4 4 0) confirms the cubic spinel structure having space group $\text{Fd}3\text{m}$ (JCPDS card no.22-1086(CoFe_2O_4) and 25-0283 (CuFe_2O_4)). The microstructural analysis is calculated for the most prominent peak (311). And the average crystallite size is calculated by Debye Scherrer formula:

$$D = \frac{0.89 \lambda}{\beta \cos \theta} \quad (1)$$

Where λ is the wavelength of the incident $\text{Cu-K}\alpha$ line of X-ray ($\lambda = 1.5418 \text{ \AA}$), β is the full width at half maximum in radians of the maximum intensity peak and θ is the angle at which the maximum peak occurs. From the micro structural analysis (table 1), the average crystallite size was found to decrease from 25 to 18 nm when the concentration of Cu increased from 0.06, 0.08 and 0.1. The decrease in the grain size with the increase in the Cu^{2+} concentration is due to the formation of Cu-O-Fe on the surface of the substituted nanoparticle that prevents further grain growth [15]. The strain and dislocation density is found to be varied accordingly. The lattice constant of $\text{Co}_{1-x}\text{Cu}_x\text{Fe}_2\text{O}_4$ is calculated by the relation [16]

$$a = d_{hkl} (h^2 + k^2 + l^2)^{\frac{1}{2}} \quad (2)$$

Where (h, k, l) are the Miller indices. It is noted that the lattice constant increases with the increase in the Cu^{2+} concentration from 0.06, 0.08 and 0.1 (table 1) and it is attributed to the occupying nature of Cu^{2+} in the position of Fe^{3+} ion and the ionic radii of copper is 0.70 \AA is greater than the ionic radii of Fe^{3+} which is 0.67 \AA . Normally the substitution of bigger ionic radii results in the peak shift and in our

case it is found so. [17, 18] Similar types of observations are noted for an increase in the annealing temperature [19]. Also, the lattice constant is found to be 8.428Å which are greater than 8.375Å, the value for bulk spinel ferrite nanoparticle. The calculated volume of the cell was less compared to the bulk [590.99Å³] which is due to the nanosizing effect in Copper substituted cobalt ferrite.

The X-ray density (ρ_x) is calculated by the relation [20]

$$\rho_x = \frac{8M}{Na^3} \quad (3)$$

Where M, the molecular mass of the compound, N, the Avogadro number (6.0225×10^{23} particles/mole) and 'a', the lattice constant. In the present case, X-ray density decreases with increase in the lattice constant which is attributed to the atomic weight of Co which is lower than Fe [21]. A similar type of observations is noted by Pandit et al for Mg-Zn ferrite system prepared at different molar concentrations [22]. Also, X-ray density is found to be higher than their bulk counterpart is due to the formation of pores during the synthesis process and ionic radii [23, 24]. The tetrahedral and octahedral ionic radii (r_A , r_B) of cubic spinel structure [25] is given by the equation

$$r_A = \left(u - \frac{1}{4}\right) a \sqrt{3} - r(O^{2-}) \text{ \AA} \quad (4)$$

$$r_B = \left(\frac{5}{8} - u\right) a - r(O^{2-}) \text{ \AA} \quad (5)$$

$r(O^{2-})$ is the radius of oxygen ion (1.35 Å); The mean ionic radius at tetrahedral site A (r_A) is found to increase slowly than the octahedral site B (r_B) which is attributed to the cation redistribution. These types of observations are noted by other investigators for their Co-Zn system [26]. The bond length (d_{AX}) and (d_{BX}) at tetrahedral and octahedral sites is given by

$$d_{AX} = \left(u - \frac{1}{4}\right) a \sqrt{3} \text{ \AA} \quad (6)$$

$$d_{BX} = \left(\frac{5}{8} - u\right) a \text{ \AA} \quad (7)$$

Where a is the lattice constant; u is the oxygen ion parameter, for ideal spinel ferrite $u=3/8$. The increase in lattice constant will reflect an increase in the tetrahedral (d_{AX}) and octahedral bond length (d_{BX}). The hopping length L_A and L_B at tetrahedral and octahedral sites is given by [25]

$$L_A = a \left(\frac{\sqrt{3}}{4}\right) \text{ \AA} \quad (8)$$

$$L_B = a \left(\frac{\sqrt{2}}{4}\right) \text{ \AA} \quad (9)$$

The structural parameters are tabulated in tables 1 and 2. It is noted that L_A and L_B increases with the decrease of grain size which is associated with an increase in the lattice constant. Also $L_A > L_B$; which shows that electron hopping is less probable between ions at tetrahedral and octahedral site than that between octahedral and octahedral sites. The tetrahedral edge ($d_{A \times E}$), shared and unshared octahedral edge ($d_{B \times E}$ and $d_{B \times EU}$) is calculated using the formula.

$$d_{AXE} = a \sqrt{2} \left(2u - \frac{1}{2}\right) \quad (10)$$

$$d_{BXE} = a \sqrt{2} (1 - 2u) \quad (11)$$

$$d_{B X E U} = a \left[4u^2 - 3u + \frac{11}{16}\right]^{\frac{1}{2}} \quad (12)$$

It is noted that the evaluated value of r_A , r_B , d_{AX} , d_{BX} , $d_{A \times E}$, $d_{B \times E}$, $d_{B \times EU}$ increases with the decrease of grain size and it is due to the cation redistribution. In the present case, the prepared samples shows ferrimagnetism. The magnetic moment of anti-parallel spins between Fe^{3+} ions at tetrahedral sites and Co^{2+} or Cu^{2+} ions at octahedral sites results in ferrimagnetism of nanoparticles. From the structural analysis it is observed that the grain size decreased as the concentration of dopant increased and corresponding changes are observed in the strain, the lattice constant, hopping length, octahedral and tetrahedral bond length etc.

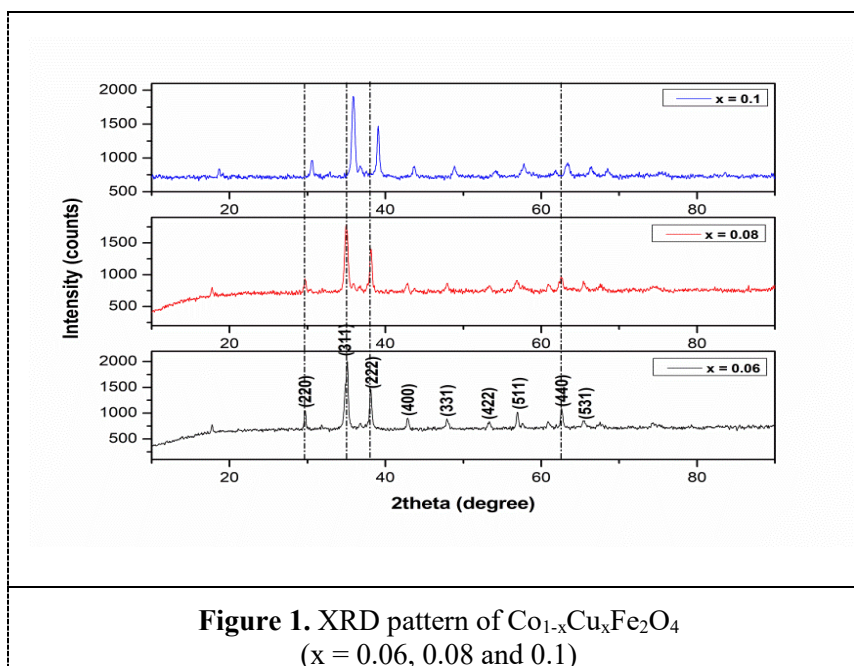


Table 1. Microstructural Parameters of $\text{Co}_{1-x}\text{Cu}_x\text{Fe}_2\text{O}_4$ ($x = 0.06, 0.08$ and 0.1)

Cu Conc. (M)	Crystallite size (nm)	Micro-strain	Lattice Constant (\AA)	X-ray density (gm cm^{-3})	r_A (\AA)	r_B (\AA)
0.06	26	0.00141	8.3024	5.4426	0.4838	0.6258
0.08	20	0.00184	8.4707	5.1247	0.5219	0.6668
0.1	18	0.00195	8.5117	5.0509	0.5313	0.6768

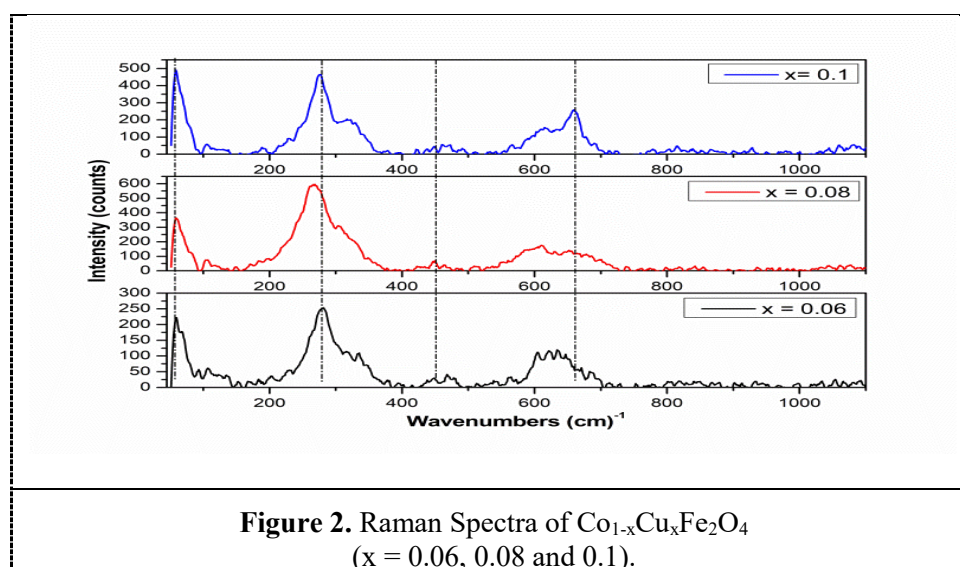
Table 2. Hopping length (d_A) and (d_B), tetrahedral edge ($d_{A \times E}$), shared ($d_{B \times E}$) and unshared octahedral edge ($d_{B \times EU}$) for $\text{Co}_{1-x}\text{Cu}_x\text{Fe}_2\text{O}_4$ ($x = 0.06, 0.08$ and 0.1)

Cu Conc. (M)	L_A (\AA)	L_B (\AA)	d_{AX} (\AA)	d_{BX} (\AA)	d_{AXE} (\AA)	d_{BXE} (\AA)	d_{BXEU} (\AA)
0.06	3.590	2.9353	1.8838	2.0270	3.7676	2.7944	2.9370
0.08	3.6679	2.9948	1.9219	2.0681	3.8439	2.8510	2.9965
0.1	3.6857	3.0093	1.9313	2.0781	3.8626	2.8649	3.011

3.2. Raman Analysis

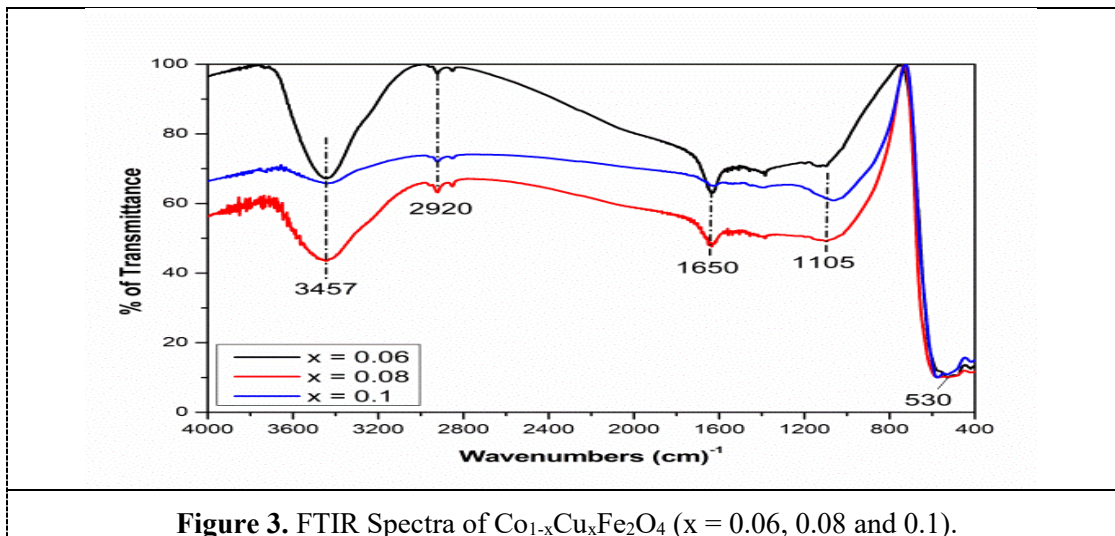
The atomic structure of $\text{Co}_{1-x}\text{Cu}_x\text{Fe}_2\text{O}_4$ ($x = 0.06, 0.08$ and 0.1) is analysed by Raman spectroscopy [27, 28] in the range $0-1100 \text{ cm}^{-1}$. The observed Raman peaks seem to be asymmetric or even dissociated. De-convolution of spectrum shows that each peak can be presented like a doublet, a characteristic of the inverse spinel structure [29]. In the present case the Raman bands (figure 2) shows a shift towards the

lower wave number side. The two most intense Raman peaks observed at 274 cm^{-1} , 466 cm^{-1} , and 660 cm^{-1} . The peaks observed at 274 cm^{-1} and 466 cm^{-1} are the characteristic modes of spinel ferrite. At the lower wavenumber range Raman mode at 660 cm^{-1} shows a shoulder like structure. This band is allocated to $A_{1g}(1)$ and $A_{1g}(2)$ modes and the low wavenumber modes are allocated to the E_g and T_{2g} modes. The mode at 466 cm^{-1} is assigned as the vibrations of the octahedral sublattices (Cu^{+2} , Fe^{+3} at B), whereas the high energy phonon mode at 660 cm^{-1} originates from vibrations of the tetrahedral sublattices (Fe^{+3} at A) [30]. The redistribution of cation doping can be noted by comparing the relative intensities of the $A_{1g}(1)$ and $A_{1g}(2)$ modes. The decrease in intensity and the peak at 660 cm^{-1} shifting towards lower wave number is due to the higher atomic mass of Cu than Co ion. The changes in the distribution of divalent and trivalent cation is due to the higher degree of cation disorders induced by the incorporation of Cu^{2+} ions and particle size effect.



3.3. Functional Group Analysis

Figure 3 shows the FTIR spectra of $\text{Co}_{1-x}\text{Cu}_x\text{Fe}_2\text{O}_4$ ($x = 0.06, 0.08$ and 0.1 M). In ferrites, each atom is covalently bonded to the nearest neighbour with same bond energies [31]. The metal ion vibrations at tetrahedral and octahedral sites are observed around 600 cm^{-1} and 400 cm^{-1} . The vibrational mode of tetrahedral clusters is higher due to the intrinsic vibration which has highest restoring force than the in-plane bending vibrations at octahedral sites. The difference in the band position is due to the difference in the distance between Fe^{3+} to O^{2-} at tetrahedral and octahedral complexes [32]. It is noted that Fe-O distance at A site is 0.198 nm which is smaller than B site is 0.199 nm [33]. In the present case, $\text{M}\leftrightarrow\text{O}$ vibrations are observed around 570 cm^{-1} . Also, a small shift in the frequency is observed when copper concentration increases which indicate the substitution of copper in the cobalt ferrite lattices [34]. The band observed at 3457 cm^{-1} and 1650 cm^{-1} is assigned to hydrogen bonded O-H group and ionic stretching of C-H bond. The band assigned at 1105 cm^{-1} is due to Co - O and Cu - O or Fe - O vibrations [35]. The existence of metal oxygen band at lower frequency confirms the existence of Co and Cu in the synthesized sample [36].



3.4. Morphological and Compositional Analysis

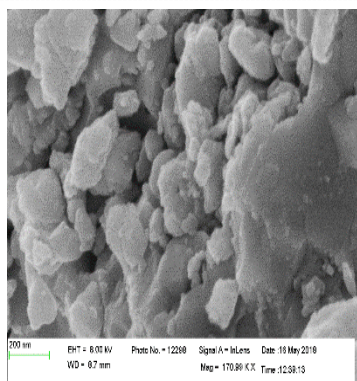


Figure 4. FESEM images of $\text{Co}_{1-x}\text{Cu}_x\text{Fe}_2\text{O}_4$ at $X = 0.06$

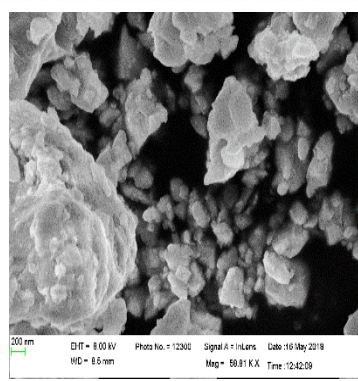


Figure 5. FESEM images of $\text{Co}_{1-x}\text{Cu}_x\text{Fe}_2\text{O}_4$ at $X = 0.08$

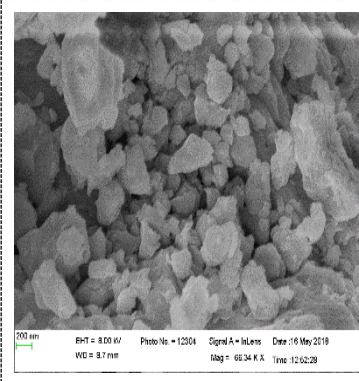


Figure 6. FESEM images of $\text{Co}_{1-x}\text{Cu}_x\text{Fe}_2\text{O}_4$ at $X = 0.1$

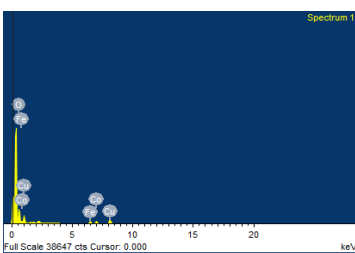


Figure 7. EDS Spectrum of $\text{Co}_{1-x}\text{Cu}_x\text{Fe}_2\text{O}_4$ at $X = 0.06$

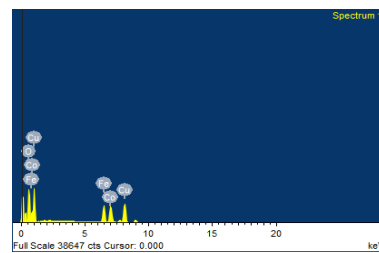


Figure 8. EDS Spectrum of $\text{Co}_{1-x}\text{Cu}_x\text{Fe}_2\text{O}_4$ at $X = 0.08$

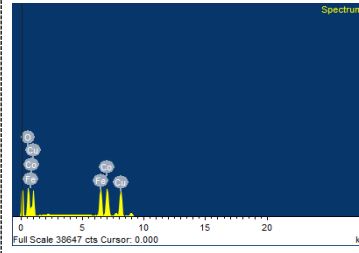


Figure 9. EDS Spectrum of $\text{Co}_{1-x}\text{Cu}_x\text{Fe}_2\text{O}_4$ at $X = 0.1$

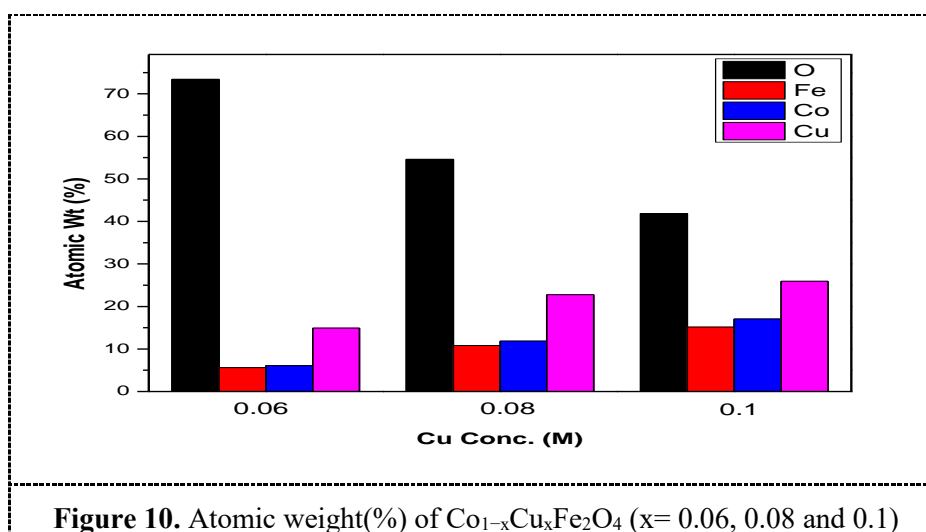


Figure 4 to 6 shows the FESEM images of Co_{1-x}Cu_xFe₂O₄ (x= 0.06, 0.08 and 0.1 M) nanoparticles. The definite shape of the particles are not visible properly and only the agglomerated particles are observed. Figure 7 to 9 shows that the EDS spectra of Co_{1-x}Cu_xFe₂O₄ (x= 0.06, 0.08 and 0.1 M) nanoparticles. The compositional analysis shows the increase in the atomic weight (%) of Cu when the copper concentration increases. It is noted that the other elements such as Co and Fe are also increased with the increase in the copper concentration (figure 10).

3.5. VSM Analysis

Magnetic hysteresis measurements for ratios 0.06, 0.08 and 0.1 M (Co_{1-x}Cu_xFe₂O₄) were taken. From the Hysteresis, it is clear that as the particle size increases, the saturation Magnetization (M_S), Retentivity(M_R) and Coercive field (H_C)increases. Figure 11 show the magnetization (emu / g) Vs magnetic induction (B) for Co_{1-x}Cu_xFe₂O₄ (x = 0.06, 0.08 and 0.1M) at room temperature. The hysteresis curve shows the variation of magnetic parameters with the increase in the copper concentration. The coercivity (H_c), remanence magnetization (M_r) and the saturation magnetization (M_s) are tabulated in table 3. In the case of ferromagnetic material, the magnetization will not pass through the origin and the hysteresis curve shows the ferromagnetic behavior of the copper substituted cobalt ferrite nanoparticle. The coercivity which is the measure of applied field at zero magnetization and remanence magnetization which is the magnetization retains by the material is shown listed in the stable [37]. In general, coercivity increases with a decrease in grain size. The narrow hysteresis loop shows ranging from 380 to 602 shows that it can be demagnetized easily [38]. From the table 3, it is noted that the coercivity and retentivity decrease with the increase in the concentration of Cu²⁺ ion from 0.06 to 0.1M which is attributed to the substitution of Cu²⁺ ion by Co²⁺ ion. The exchange interaction between the substituted ion and existing ion results in decrease in saturation magnetization. As the electron spins at A (tetrahedral) sites and B (octahedral) sites are antiparallel and nullify each other. But the spins within A and B sites are parallel and hence the total magnetization of the material is attributed to the magnetic effect of B sites. When the nonmagnetic Cu²⁺ ion is substituted for Fe³⁺ ion in the A site, the total unpaired electrons in the B site increases which result in increased saturation magnetization. The substitution of nonmagnetic Cu²⁺ ion in the position of B site results in decrease in saturation magnetization which reduces the interaction between A and B sites [39, 40]. The superexchange interaction between A-A, B-B and A-B sites is depends on the chemical composition. The preferential site of Cu²⁺ is A site than in the B site and hence the Co²⁺ from A site slowly shifted results in weakening of B-B interaction and this results in a decrease in the saturation magnetisation when the copper concentration increases [41]. The remanence ratio M_r/M_s also varies with the copper concentration (0.06, 0.08 and 0.1 M) with initially increases and then decreases.

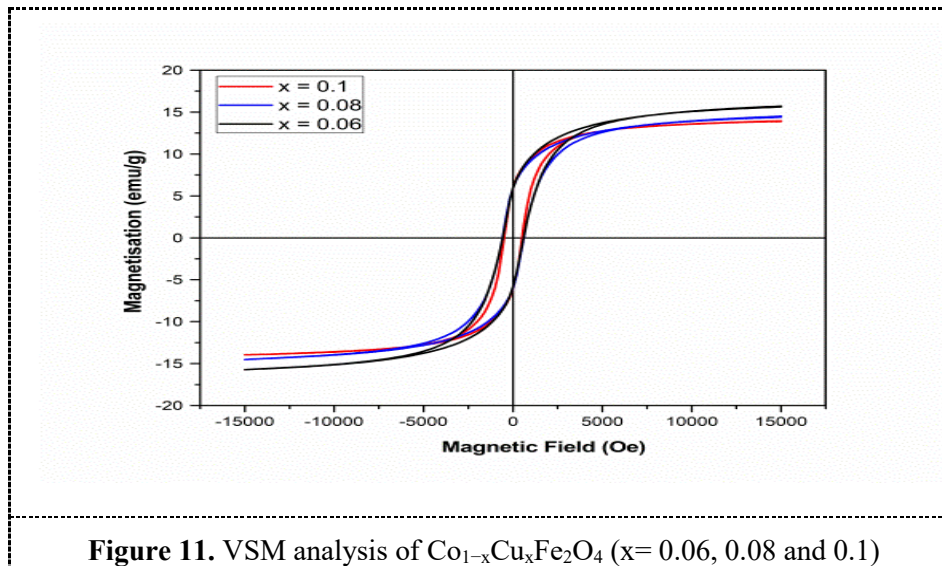


Table 3. Magnetic Parameters of $Co_{1-x}Cu_xFe_2O_4$ ($x= 0.06, 0.08$ and 0.1 M)

Cu Conc. (M)	Coercivity (Oe)	Mr (emu/g)	Ms (emu/g)	Mr / Ms
0.06	602.64	5.942	14.25	0.41
0.08	450.91	5.710	13.67	0.42
0.1	380.94	3.260	8.23	0.40

4. Conclusion

Copper Substituted Cobalt Ferrite nanoparticles were synthesized by Sol-Gel auto combustion technique varying the citric acid to metal nitrate by volumetric ratio. The microstructural analysis confirms cubic spinel phase structure of the prepared samples and the average crystallite size decreases from 25nm to 18nm with an increase in the ratio of metal nitrate to citric acid from 1:2 to 1:4. The most profound decrease was found when the volumetric ratio changes from 1:2 to 1:3. In the case of Copper substituted $CoFe_2O_4$, the Raman bands showed a shift towards the lower wavenumber, which are Raman active bands in Fe_3O_4 all the tetrahedral and octahedral sites are occupied by Fe ions while in $CoFe_2O_4$ the octahedral sites are occupied either by Co or Fe ions. Intensity decrease of 660 cm^{-1} tetrahedral Raman band and all the peaks are shifted towards the lower wavenumber side due to a higher atomic mass of Cu compared to the Co ion. As in spinel ferrite, the distribution of divalent and trivalent cations can be changed due to the migration of metal ions from tetrahedral to octahedral sites and vice versa. These changes could be due to a high degree of cation disorder induced by incorporation of Cu^{2+} ion or a particle size effect. From the FTIR analysis, the band observed at 3457 cm^{-1} and 1650 cm^{-1} is assigned to hydrogen bonded O-H group and ionic stretching of C-H bond. The band assigned at 1105 cm^{-1} is due to Co - O and Cu - O or Fe - O vibrations. The presence of Co and Cu confirms by the metal oxygen band at lower frequency. The morphological and compositional analysis was done which confirmed the increase in copper concentration in the sample. The magnetic studies revealed that as the ratio of metal nitrates increases, the coercivity, saturation magnetization, and remanence decreases following a hysteresis path. So, by the above characterization technique, we were successfully able to confirm the substitution of Copper in the tetrahedral sites of Cobalt Ferrite. The project also yielded effective results in using transition metals as substituted metal nitrates for controlling the size of the nanoparticle.

References

- [1] Sugimoto M 1999 *J. Am. Ceram. Soc.* **82** 269
- [2] Jamon D, Donatini F, Sibli A, Royer F, Perzynski R, Cabuil V, and Neveu S 2009 *J. Magn. Magn. Mater.* **321** 1148
- [3] Zhen L, He K, Xu C Y, and Shao W Z 2008 *J. Magn. Magn. Mater.* **320** 2672
- [4] Pileni M P 2001 *Adv. Funct. Mater.* **11** 323
- [5] Liu C, Zou B, Rondinone A J, and Zhang Z J 2000 *J. Phys. Chem. B.* **104** 1141
- [6] Katz E, Shipway A N, Willner I 2005 *Nanoparticles* (Wiley-VCH Verlag GmbH & Co. KGaA)
- [7] Noppakun Sanpo, James Wang, and Christopher C. Berndt 2013 *Journal of Nano Research* **22** 95
- [8] Yang Y, Jing L, Yu X, Yan D, Gao M 2007 *Chem. Mater.* **19** 4123
- [9] Liu M, Li X, Imrane H, Chen Y, Goodrich T, Cai Z, Ziemer K S, Huang Y, Sun N X 2007 *Appl. Phys. Lett.* **90** 152501
- [10] Plank N O V, Snaith H J, Ducati C, Bendall J S, Schmidt-Mende L, Welland M E 2008 *Nanotechnology* **19** 465603
- [11] Yanez-Vilar S, Sanchez-Andujar M, Gomez-Aguirre C, Mira J, Senaris-Rodriguez M A, Castro-Garcia S 2009 *J. Solid State Chem.* **182** 2685
- [12] Maaz K, Mumtaz A, Hasanain S K, Ceylan A 2007 *J. Magn. Magn. Mater.* **308** 289
- [13] Hu X G and S.J. Dong S J 2008 *J. Mater. Chem.* **18** 1279
- [14] Salunkhe A B, Khot V M, Phadatare M R, Pawar S H 2012 *Alloys Compds.* **514** 91
- [15] Alireza Samavati and Ismail A F 2017 *Particuology* **30** 158
- [16] Saccone F D, Ferrari S, Errandonea D, Grinblat F, Bilovol V and Agouram 2015 *Journal of Applied Physics* **118** 075903.
- [17] Hashim M, Alimuddin Kumar S, Koo B H, Shirsath S E, Mohammed E M, Shah J, Kotnala R K, Choi H K, Chung H and Ravikumar 2012 *J. Alloy. Compd.* **518** 11
- [18] Balavijayalakshmi J, Suriyanarayanan N, Jayaprakash R 2012 *Mater. Lett.* **81** 52
- [19] Raghvendra Singh Yadav, Ivo Kuřitka, Jarmila Vilcakova, Jaromir Havlica, Jiri Masilko, Lukas Kalina, Jakub Tkacz, Jiří Švec and Vojtěch Enevand Miroslava Hajdúchová 2017 *Nanoscience and Nanotechnology* **045002** 14.
- [20] Rahman M D T, Vargas M and Ramana C V 2014 *J. Alloys and Comp.* **617** 547
- [21] Kittel C 2004 *Introduction to Solid State Physics* (John Wiley & Sons, Inc)
- [22] Pandit A, Shitre A R, Shengule D R and Jadhav K M 2005 *J. Mater. Sci.* **40** 423
- [23] Muhammad and Maqsood A 2008 *J. Alloy. Com.* **460** 54
- [24] Abbas T, Islam M U, Ashraf M Ch 1995 *Modern Phys. Lett. B.* **9** 1419
- [25] Nikam D S, Jadhav S V, Khot V M, Bohara R A, Hong C K, Mali S S and Pawar S H 2015 *RSC Adv.* **5** 338.
- [26] Deraz N M and Alarifi A 2012 *Journal of Analytical and Applied Pyrolysis* **97** 55
- [27] Baraliya J D and Joshi H H 2014 *Vib. Spectrosc.* **74** 75
- [28] Liu B H and Ding J 2006 *J. Phys. Chem. B* **88** 042506
- [29] Ahlawat A and Sathe V G 2011 *J. Raman Spectrosc.* **42** 1087.
- [30] Liu W, Chan Y, Cai J, Leung C, Mak C, Wong K, Zhang F, Wu X, and Qi X D 2012 *J. Appl. Phys.* **112** 104306
- [31] Waldron R 1955 *Physical Review* **99** 1727
- [32] Labde B, Sable M C and Shamkuwar N 2003 *Materials letters* **57** 1651
- [33] Gabal N, A I A Nagri Y and Kadai N 2011 *Polyhedron* **30** 1185
- [34] Sattar A, E I – Sayed H, E I – Shokrofy K and EI – Tabey M 2005 *Journal of Applied Science* **3** 162
- [35] Rakesh K Singh, Rai B C and Prasad K (2012) *International Journal of Advance Material Science* **3** 71
- [36] Markov – Denevai 2012 *Journal of Uni. Chem. Technol. Metall.* **45** 351
- [37] Ansari F, Sobhani A and Salavati-Niasari M 2014 *RSC Adv.* **4** 63946

- [38] Shadab Dabagh, Alia Ati, S K Ghoshal, Samad Zare, R M Rosnan, Ahmed S Jbara and Zulkafli Othaman 2016 *Bulletin of Material Science*, **39** 1029
- [39] Hashim M, Alimuddin, Kumar S, Koo B H, Shirsath S E, Mohammed E M, Shah J, Kotnala R K, Choi H K, Chung H, Ravikumar 2012 *J. Alloy. Compd.* **518** 11
- [40] Neel L 1948 *Ann. Phys. Paris.* **3** 137
- [41] Sharifi I, Shokrallahi H, Doroodmann M, Safi R 2012 *J. Magn. Magn. Mater.* **324** 1854